

Appearance of c -axis magnetic moment in odd-parity antiferromagnetic state in CeRh_2As_2 revealed by ^{75}As -NMR

Shiki Ogata,^{1,*} Shunsaku Kitagawa,¹ Katsuki Kinjo,² Kenji Ishida,¹ Manuel Brando,³ Elena Hassinger,^{3,4} Christoph Geibel,³ and Seunghyun Khim³

¹*Department of Physics, Kyoto University, Kyoto 606-8502, Japan*

²*Institute of Multidisciplinary Research for Advanced Materials, Tohoku University, Sendai, Miyagi 980-8577, Japan*

³*Max Planck Institute for Chemical Physics of Solids, D-01187 Dresden, Germany*

⁴*Technical University Dresden, Institute for Solid State and Materials Physics, D-01062 Dresden, Germany*

(Dated: December 16, 2024)

CeRh_2As_2 shows the superconducting (SC) multiphase under the c -axis magnetic field, which is considered to originate from local inversion symmetry breaking at the Ce site. We reported that the antiferromagnetic (AFM) order is inside the SC phase and that the AFM state disappears at the transition field to the high-field SC phase. However, the magnetic structure in the AFM state has not been clarified yet. In this study, we performed ^{75}As -NMR measurements in the SC phase in $H \parallel [110]$ to identify the magnetic structure. Comparing the NMR linewidth with $H \parallel c$, we found that the internal magnetic field is oriented to the c axis. This suggests a $\mathbf{q} = \mathbf{0}$ A -type AFM with the moments parallel to the c axis. We also observed the reduction of the spin susceptibility, which indicates spin-singlet superconductivity in the low-field SC phase. This study provides an important clue to clarify the correlation between the SC multiphase, magnetism, and local inversion symmetry breaking.

PACS numbers: 74

I. INTRODUCTION

In conventional superconductors, magnetism and superconductivity are incompatible with each other. In strongly correlated electron systems, on the other hand, superconductivity is often realized near the magnetic ordered phase and the maximum superconducting (SC) transition temperature T_{SC} is achieved at the quantum critical point [1–4]. In such superconductors, magnetic fluctuations are considered to be the origin of pair formation [5–7]. Therefore, it is extremely important to investigate the relationship between magnetism and superconductivity to identify the mechanism of superconductivity.

CeRh_2As_2 is a recently discovered heavy-fermion superconductor with $T_{\text{SC}} \sim 0.3$ K [8]. The crystal structure of CeRh_2As_2 is of tetragonal CaBe_2Ge_2 type with the space group $P4/nmm$ (No. 129, D_{4h}^7). There are two crystallographically inequivalent As and Rh sites; As(1) [Rh(1)] is tetrahedrally coordinated by Rh(2) [As(2)], as shown in Fig. 1(a). The H - T phase diagram in $H \parallel c$ is quite unusual, showing a clear SC multiphase, while a single SC phase in $H \parallel [110]$. This SC multiphase is quite similar to the theoretically proposed pair-density-wave (PDW) state originating from the locally broken inversion symmetry at the SC layers [9]. This PDW state is intriguing, in which the odd-parity superconductivity with only the spin-singlet SC order parameter is expected to be realized. The PDW state is suggested to exhibit

topological superconductivity [10] and unique responses owing to the SC parity transition [11, 12]. CeRh_2As_2 was also reported to exhibit a nonmagnetic phase transition at $T_0 \sim 0.4$ K just above T_{SC} [8, 13–16]. Although the specific-heat jump at T_{SC} is large, the anomaly at T_0 is rather weak. This transition is considered as an electric quadrupole density-wave (QDW) order of the quasi-quartet state consisting of ground and excited doublets coupled by the Kondo effect [13, 17]. In addition to the QDW state, the in-plane antiferromagnetic (AFM) state [18] and polarized charge distributions of Ce^{3+} ions [19] have been discussed as the order parameters below T_0 . However, there are few experimental reports about order parameters below T_0 , making it still an open question.

In addition to the SC multiphase and QDW phase, AFM order at $T_{\text{M}} < T_{\text{SC}}$ was suggested by our nuclear quadrupole resonance (NQR) measurement [20]. This AFM order is realized in the low-field SC phase, and it disappears almost simultaneously with the transition to the high-field SC phase [21]. The interplay between the SC multiphase and the AFM state in CeRh_2As_2 has also been studied theoretically [22–24]. In recent higher-quality single crystals, a first-order transition below T_{SC} has also been reported in the specific heat measurement [25]. On the other hand, recent specific-heat [25] and muon spin relaxation (μSR) measurements [26] using higher-quality samples suggested that magnetic order emerges from T_0 , indicating that there are still unresolved aspects regarding the magnetic phase. In any case, CeRh_2As_2 is a promising candidate to study the unconventional nonmagnetic, AFM, and SC states as well as their interplays, originating from locally broken inversion symmetry. However, the magnetic structure in the AFM

* ogata.shiki.86c@st.kyoto-u.ac.jp

state has not been determined, and the behavior of the SC and AFM phases in $H \parallel [110]$ has not been investigated. Hence, a detailed study of the magnetic state was desired.

While the bulk magnetic susceptibility is hindered by the SC diamagnetic shielding effect, nuclear magnetic resonance (NMR) can measure the spin susceptibility in the SC state. In addition, NMR is sensitive to the internal magnetic field at the observed nuclear sites, so the magnetic structure can be discussed by comparing the internal magnetic field at different nuclear sites. In fact, the cancellation of the internal magnetic field at the As(1) site in the NQR measurements [20] leads to two possible magnetic structures: the A -type AFM (in-plane ferromagnetic and inter-plane antiferromagnetic) state with magnetic moments parallel to the c axis or the helical state with in-plane moments [$\mathbf{q} = (\pi, \pi, \pi)$]. Therefore, NMR is one of the most powerful techniques to investigate the SC and magnetic properties.

In this paper, we report the ^{75}As -NMR results of CeRh_2As_2 in $H \parallel [110]$. We observed the reduction of the spin susceptibility in the SC state, ensuring our previous report of the formation of spin-singlet pairing in the low-field SC state. This is because the possibility of spin-triplet pairing still remained if the spin susceptibility perpendicular to the c axis was not measured. The field distribution at the As(2) site is smaller than that in $H \parallel c$ [21], indicating that the internal magnetic field at the As(2) site is parallel to the c axis. From this result, we propose a $\mathbf{q} = \mathbf{0}$ A -type magnetic structure in the AFM state. This paper provides essential insights into the interplay between magnetism and superconductivity in locally inversion symmetry breaking systems.

II. EXPERIMENTAL

Single crystals of CeRh_2As_2 were grown using the bismuth flux method [8]. Although high quality CeRh_2As_2 single crystals have recently been reported [15, 27], the sample used in this paper is the same early stage sample as in our previous study [20, 21, 28, 29]. The magnetic field dependence of T_{SC} was determined from the second-order derivative of the SC diamagnetic signal with the ac susceptibility measurements using an NMR coil as shown in Fig.1(b). For the NMR measurements, we used a split SC magnet that generates a horizontal field and combined it with a single-axis rotator to apply a magnetic field parallel or perpendicular to the c axis. Low-temperature NMR measurements down to 0.06 K were performed using a ^3He - ^4He dilution refrigerator, in which the sample was immersed in the ^3He - ^4He mixture to reduce radio-frequency heating during measurements. A conventional spin-echo technique was used for the NMR measurements. The magnetic field was calibrated using ^{63}Cu (nuclear gyromagnetic ratio $^{63}\gamma_n/2\pi = 11.289$ MHz/T) and ^{65}Cu ($^{65}\gamma_n/2\pi = 12.093$ MHz/T) NMR signals from the NMR coil. We experi-

mentally confirmed superconductivity immediately after the NMR pulses using a technique reported in previous studies [30, 31]. The ^{75}As -NMR spectra (nuclear spin $I = 3/2$, $\gamma/2\pi = 7.29$ MHz/T, and natural abundance 100%) were obtained as a function of frequency at fixed magnetic fields. Reflecting two crystallographically inequivalent As sites, two ^{75}As -NMR peaks were observed in all measurement ranges as shown in Figs. 2(a) and 2(b). The site assignment of the NMR peaks was described in a previous paper [28].

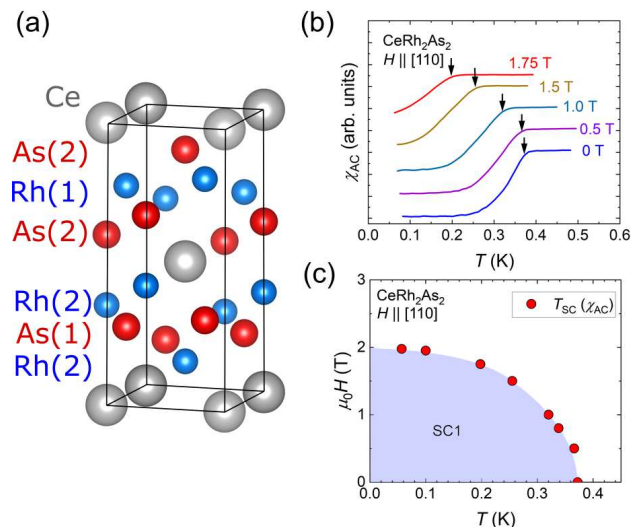


FIG. 1. (a) Crystal structure of CeRh_2As_2 [32]. (b) Temperature dependence of ac susceptibility measurements in $H \parallel [110]$. The black arrows indicate the superconducting transition temperature T_{SC} estimated from the peak of the second-order derivative. (c) H - T phase diagram under $H \parallel [110]$.

III. RESULTS

To investigate the SC and magnetic properties, particularly the magnetic structure in the AFM state, we performed ^{75}As -NMR measurements of two As sites. As shown in Figs. 2(a) and 2(b), the NMR frequencies of 0.6 K at $\mu_0 H \sim 0.8$ T were $f^{\text{As}(1)} \sim 11.55$ MHz and $f^{\text{As}(2)} \sim 9.56$ MHz, respectively. [See Figs. 4(a) and 4(b) for details of the transition.] The sharp spectrum of ^{65}Cu -NMR from a NMR coil was also observed. The full width at half maximum (FWHM) and the resonance frequency were determined by the fitting, shown with the dashed lines in Figs. 2(a) and 2(b). As for the fitting, we adopted a Gaussian function for the As(1) site and a Lorentzian function for the As(2) site as the fitting function based on the shape of the NMR spectra. Although a theoretical paper predicted the stripe-AFM order at T_0 [18], we did not find any change both in the Knight shift and FWHM within the resolution at T_0 . At low tempera-

tures, the spectrum of the As(1) site became asymmetric. Thus, we used an asymmetric Gaussian function with an asymmetrization factor α : $\frac{1}{\sqrt{2\pi}w} \exp\left[-\frac{(x-\mu)^2}{2[w+\alpha(x-\mu)]^2}\right]$ [33]. Such asymmetric broadening may be caused by an internal field at the As(1) site, for example, field-induced ferromagnetic components with the AFM state. Since the hyperfine coupling constant of the As(1) site is negative in $H \parallel [110]$, ferromagnetic components broaden the NMR spectra in the low-frequency direction. We adopted the peak frequency as the Knight shift, and estimated the Knight shift by numerical calculations with a diagonalized nuclear Hamiltonian. Below T_{SC} , the NMR spectra broaden due to SC diamagnetism. However, a significant site-dependent broadening, observed in $H \parallel c$ below 0.25 K [21], was not observed in $H \parallel [110]$. The Knight shifts for the As(1) and As(2) sites are denoted by $K^{As(1)}$ and $K^{As(2)}$ in Fig. 2(d), respectively. In the normal state, the Knight shifts of both sites are constant below 1 K. Below T_{SC} , $K^{As(2)}$ decreased, but $K^{As(1)}$ slightly increased. Note that the hyperfine coupling constant $A_{hf,[110]}$ of the As(1) site is negative while that of the As(2) site is positive [29], thus we can say that we observed a decrease of the spin susceptibility at both sites in the SC state. Considering that the spin susceptibility also decreases in $H \parallel c$ [21], this indicates that $CeRh_2As_2$ is in the spin singlet pairing in the low-field SC state.

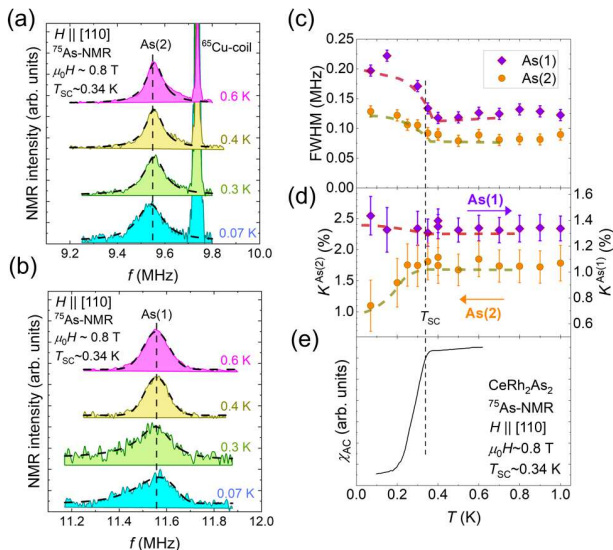


FIG. 2. NMR measurements in $CeRh_2As_2$. The temperature evolution of the NMR spectra of (a) the As(1) site and (b) the As(2) site at 0.8 T for $H \parallel [110]$. The dashed vertical lines indicate the NMR frequency of the normal-state signal. The dashed curves indicate the results of a fitting. Temperature dependence of (c) full width at half maximum (FWHM), (d) Knight shift at the As(1) site $K^{As(1)}$, and As(2) site $K^{As(2)}$ determined by the NMR spectrum at 0.8 T. T_c is indicated by the black dashed line. The colored dashed lines in (c) and (d) are guides to the eye. (e) Temperature dependence of ac magnetic susceptibility at 0.8 T for $H \parallel [110]$.

From the obtained NMR spectra, we estimated the magnetic field distribution $\Delta\mu_0 H$ at each As site arising from the staggered internal field in the AFM state. In $H \parallel [110]$, the effect of the nuclear quadrupole interaction cannot be ignored unlike the case of the central peak ($1/2 \leftrightarrow -1/2$ transition) in $H \parallel c$. Therefore, we used the slope of the resonance frequency against the magnetic field obtained by numerical calculations with a diagonalized nuclear Hamiltonian as shown in Fig. 3(a). From the slope, the effective gyromagnetic ratio at each site is estimated as 13.47 MHz/T for the As(1) site and 3.33 MHz/T for the As(2) site in the measurement field region, respectively. Using this coefficient, the increase of FWHM in the SC state is converted to the increase of the magnetic field distribution $\Delta\mu_0 H$, as shown in Fig. 3(b). The result of the central peak in $H \parallel c$ in the previous study [21] is also shown in Fig. 3(c).

IV. DISCUSSION

Comparing the result in $H \parallel [110]$ and $H \parallel c$, we determine the orientation of the internal field in the AFM state. The staggered internal field in the AFM state causes the splitting of the NMR spectra in principle, and makes the spectra broaden in observation. Here, the broadening (or splitting) by the internal field depends on the orientation relative to the applied field; the broadening is largest when the internal field is parallel to the applied field. As is clear from Figs. 3(b) and 3(c), the field distribution $\Delta\mu_0 H$ at the As(2) site is larger in $H \parallel c$, while that at the As(1) site is almost the same in both field directions. This indicates that the internal magnetic field at the As(2) site is oriented to the c axis and the magnitude is around 16 mT, which is estimated from half of the difference of the field distribution between the two As sites in $H \parallel c$. The magnetic structures, in which the internal magnetic field cancels at the As(1) site, are pinned down to the two magnetic structures, as discussed in Ref. [20]. In these two structures, the one shown in Fig. 3(d) is the most plausible structure, considering the orientation of the internal magnetic field at the As(2) site. Thus, we propose that the magnetic structure is the $\mathbf{q} = \mathbf{0}$ A -type AFM state with magnetic moments $\mu \parallel c$. Using the hyperfine coupling constant of the As(2) site in $H \parallel c$ (~ 0.27 T/ μ_B) [28, 29], the ordered moment is estimated to be on the order of 0.1 μ_B . Note that the field distribution at the As(2) site in the zero-field NQR at the lowest temperature (0.1 K) [20] is larger than that in the c -axis 1.2 T NMR (0.07 K) [21], suggesting that the magnetic moment is reduced by the c -axis field. Such a small ordered moment is consistent with the absence of the static magnetic scattering in elastic neutron diffraction measurements [34]. Here, in systems with small magnetic anisotropy, the direction of the staggered moments is expected to reorient perpendicular to the c axis under the c -axis field. In such cases, however, the increase of the field distribution of 16 mT re-

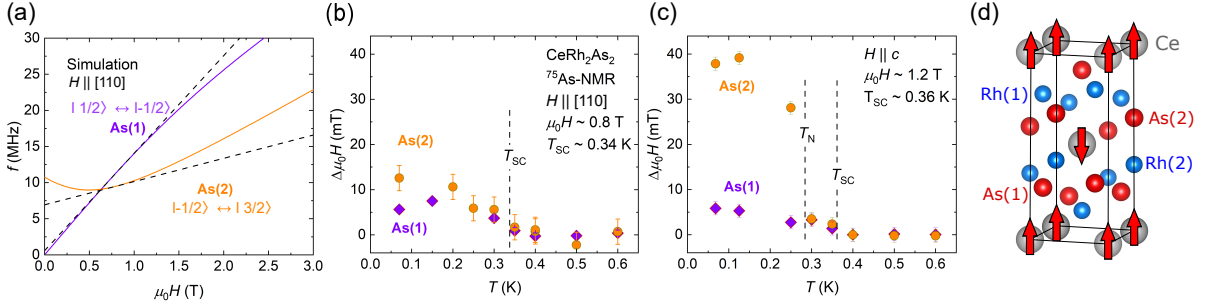


FIG. 3. (a) Magnetic field dependence of NMR frequency of each As site obtained from NMR spectrum simulation. The dashed lines indicate the result of linear fitting at 0.8 T. (b) The temperature dependence of the field distribution at As sites at 0.8 T for $H \parallel [110]$ estimated from simulation. (c) The temperature dependence of the field distribution at As sites at 1.2 T for $H \parallel c$ (estimated from Ref. [21]). (d) The possible magnetic structure with $H_{int} \parallel c$ at the As(2) site.

quires a ten times larger ordered moment ($\sim 1\mu_B$), which is inconsistent with the low-temperature linewidth of the NQR spectra [20]. It is noted that this magnetic structure seems to be incompatible with the anisotropy of the spin susceptibility in the normal state and the presence of the two-dimensional (2D) XY -type AFM fluctuation [28, 34]. It is considered that the orientation of the ordered moments is determined by the spin-orbit coupling or the interaction between magnetic moments. Since this study was performed on an early stage sample, it is important to measure the sample dependence using the recently reported higher-quality samples [15, 27].

Certain AFM states in the locally inversion symmetry breaking crystals break global inversion symmetry, which are called odd-parity multipolar states [35–38]. In fact, the $\mathbf{q} = \mathbf{0}$ A -type AFM state with $\mu \parallel c$ is equivalent to the case of the magnetic monopole order [36, 37]. Cross-correlated responses such as the electromagnetism effect are expected in the magnetic monopole order [38]. Superconductivity coexisting with odd-parity multipoles is very rare. Therefore, CeRh_2As_2 provides a promising platform to study the relationship between superconductivity and unconventional multipoles.

Next, we discuss the change in the Knight shift below T_{SC} . In a conventional spin-singlet superconductor, the spin susceptibility decreases and becomes almost zero at $T \rightarrow 0$ K due to the disappearance of the electron spin degrees of freedom as a pair formation. The spin susceptibility can be obtained from the Knight-shift measurement, but the Knight shift also includes a temperature-independent orbital component associated with Van-Vleck susceptibility, and the SC diamagnetic effects. Therefore, the temperature dependence of the observed Knight shift ΔK can be divided into the following three contributions,

$$\Delta K = K_{\text{normal}} + \delta K_{\text{spin}} + K_{\text{dia}}, \quad (1)$$

where K_{normal} is the temperature dependent Knight shift in the normal state, δK_{spin} is the change in the spin component of the Knight shift ascribed to the pair formation, and K_{dia} is the SC diamagnetic component. In the SC

state, the Knight shift decreases due to the SC diamagnetic shielding effect, and the value at 0 K is approximately expressed as [39]

$$K_{\text{dia}} = -\frac{H_{c1}}{H} \frac{\ln\left(\frac{\beta\lambda_d}{\sqrt{e}\xi}\right)}{\ln\kappa}. \quad (2)$$

Here, H_{c1} is the lower critical field, ξ is the Ginzburg-Landau (GL) coherence length, β is a factor that depends on the vortex structure and is 0.38 for the triangular vortex lattice, λ_d is the distance between the vortices and is calculated using the relation $\phi_0 = \frac{\sqrt{3}}{2}\lambda_d^2(\mu_0 H_{\text{ext}})$, e is Euler's number, and κ is the GL parameter. From the orbital limiting field $\mu_0 H_{\text{orb}} \sim 8$ T, and the thermodynamic critical field $\mu_0 H_c = 31$ mT [8], $\mu_0 H_{c1} = 0.625$ mT, $\xi = 6.42$ nm, and $\kappa = 182$ were adopted. At the measured magnetic field of $\mu_0 H \sim 0.8$ T, K_{dia} is estimated to be around 0.01%. Despite this value being several times smaller than the error bar of the measurement and does not have a significant impact in the study, this value is subtracted from here on.

To quantitatively discuss the reduction of the Knight shifts in Fig. 2(d), we compared H_{c2} with the Pauli-limiting field H_P estimated from the change in the Knight shift as follows. In a heavy-fermion spin-singlet superconductor, H_{c2} in the low temperature region is determined by the magnetic field where the energy gain by Zeeman-splitting effect is as high as the SC condensation energy: It is called the Pauli depairing effect. It is well known that the Pauli limiting field H_P for spin-singlet superconductors is expressed by the following simple equation with the decrease in the spin susceptibility $\delta\chi$ ascribed to singlet-pair formation:

$$\frac{1}{2}\delta\chi \mu_0 H_P(0)^2 = \frac{1}{2}\mu_0 H_c^2. \quad (3)$$

This equation yields $\mu_0 H_P(0) = \mu_0 H_c / \sqrt{|\delta\chi|}$, where $\delta\chi$ can be estimated from δK_{spin} as $\delta\chi = A_{\text{hf}}\delta K_{\text{spin}}$. When we assume that superconductivity in $H \parallel [110]$ is destroyed by the Pauli depairing effect, we evaluate the

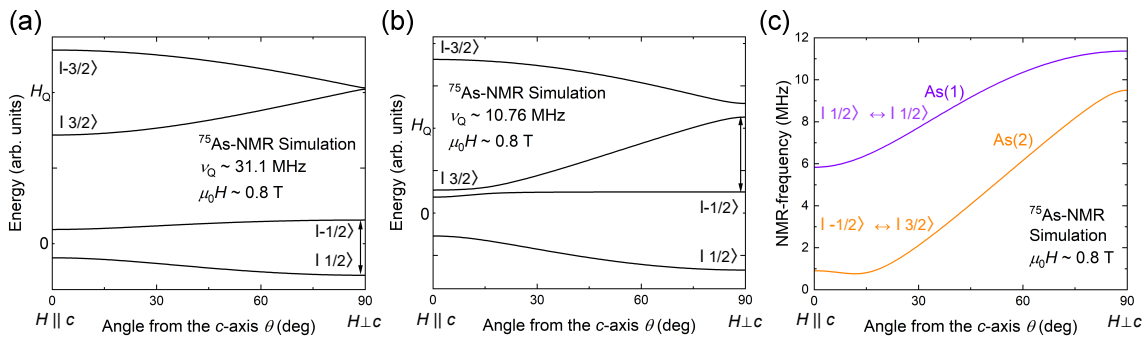


FIG. 4. The polar angle θ dependence of the energy level of the ^{75}As nuclear spin simulated by diagonalizing nuclear Hamiltonian for (a) the As(1) site and (b) the As(2) site. $H_Q = h\nu_Q$ is the energy of the nuclear quadrupole interaction ($H = 0$). The arrows represent the transitions observed in the experiment. (c) θ dependence of the NMR frequency at each As site.

corresponding Knight-shift reduction to be $\delta K_{\text{spin}}^{\text{As}(1)} \sim -0.04\%$ (slightly increase) and $\delta K_{\text{spin}}^{\text{As}(2)} \sim 0.03\%$, respectively. Thus, for the As(1) site, δK_{spin} is the same order as the error bar, but for the As(2) site, experimental $\delta K_{\text{spin}} \sim 0.4\%$ is one order larger than the estimation. Therefore, the resonance frequency of the As(2) site might decrease by an effect other than the decrease associated with the SC spin susceptibility.

Here, we consider the origin of the large reduction of $K^{\text{As}(2)}$. In the above discussion, we assumed that the change in NMR frequency is totally due to that in the Knight shift, but change in NQR frequency ν_Q and the internal magnetic field also shift the resonance frequency. However, it was suggested that the temperature evolution of ν_Q was negligibly small [20], and thus we consider the effect of the internal magnetic field in the AFM state. As shown in Fig. 3(d), the internal field at the As(1) site cancels out, which is in good agreement with the fact that a large ΔK is observed only at the As(2) site. The magnitude of the effective field at the nucleus, $H_{\text{eff}} = \sqrt{H_{\text{int}}^2 + H_{\text{ext}}^2}$, is almost the same as that of the external field H_{ext} when the internal field H_{int} is small. However, the direction of H_{eff} is slightly tilted to the c axis due to the appearance of the internal field along the c axis, which can change the resonance frequency of the As(2) site. Figure 4 shows the polar angle θ dependence of the nuclear level and NMR frequency simulated by diagonalizing the nuclear Hamiltonian. As can be seen in Fig. 4(c), the NMR frequency at the As(2) site decreases as H_{eff} shifts from $H \perp c$. When we adopt that the internal magnetic field at the As(2) site is 16 mT along the c axis, the resonance frequency decreases by 11.5 kHz, corresponding to $\Delta K \sim 0.43\%$. Thus, it is noted that the effect of the internal magnetic field is involved in the overestimation of the Knight shift.

V. CONCLUSION

We performed ^{75}As -NMR measurements on CeRh_2As_2 in order to investigate the in-plane spin susceptibility in the low-field SC state and the direction of the internal magnetic field in the AFM state coexisting with superconductivity. By combining with previous results, the spin susceptibility in all directions decreases in the SC state, indicating a spin-singlet state. The excess decrease in the Knight shift at the As(2) site in $H \parallel [110]$ could be interpreted as the effect induced by the internal magnetic field along the c axis. In addition, the field distribution due to the internal magnetic field at the As(2) site is much smaller than that in $H \parallel c$, suggesting that the internal magnetic field is oriented to the c axis. We point out the possible magnetic structure shown in Fig. 3(d) by considering it together with the cancellation of the internal magnetic field at the As(1) site. Quite recently, μSR measurements detected a static field below T_0 , which has comparable in-plane and c -axis components with a weakly anisotropic magnetic structure [26]. This seems to be different from our NMR structure, but the sample quality and experimental conditions are different between the NMR and μSR measurements. Further experiments are needed to settle the issue. In any cases, our results should be fundamental for clarifying the relationship between the field-induced SC multiphase and the magnetism in CeRh_2As_2 .

ACKNOWLEDGMENTS

This work was partially supported by the Kyoto University LTM Center and Grants-in-Aid for Scientific Research (KAKENHI) (Grants No. JP19K14657, No. JP19H04696, No. JP20KK0061, No. JP20H00130, No. JP21K18600, No. JP22H04933, No. JP22H01168, and No. JP23H01124, No. JP23K19022, and No. JP24KJ1360). This work was also supported by JST

SPRING (Grant No. JPMJSP2110) and research support funding from the Kyoto University Foundation, and ISHIZUE 2024 of Kyoto University Research Department Program, and Murata Science and Education Foundation. C. G. and E. H. acknowledge support from the DFG

program Fermi-NESt through Grant No. GE 602/4-1. Additionally, E. H. acknowledges funding by the DFG through CRC1143 (Project No. 247310070) and the Würzburg-Dresden Cluster of Excellence on Complexity and Topology in Quantum Matter—ct.qmat (EXC 2147, Project ID 390858490).

-
- [1] S. Araki, M. Nakashima, R. Settai, T. C. Kobayashi, and Y. Onuki, *Pressure-induced superconductivity in an antiferromagnet $CeRh_2Si_2$* , J. Phys.-Condens. Matter **14**, L377 (2002).
- [2] T. Park, F. Ronning, H. Q. Yuan, M. B. Salamon, R. Movshovich, J. L. Sarrao, and J. D. Thompson, *Hidden magnetism and quantum criticality in the heavy fermion superconductor $CeRhIn_5$* , Nature **440**, 65 (2006).
- [3] O. Trovarelli, M. Weiden, R. Müller-Reisener, M. Gómez-Berisso, P. Gegenwart, M. Deppe, C. Geibel, J. G. Sereni, and F. Steglich, *Evolution of magnetism and superconductivity in $CeCu_2(Si_{1-x}Ge_x)_2$* , Phys. Rev. B **56**, 678 (1997).
- [4] S. Kasahara, T. Shibauchi, K. Hashimoto, K. Ikeda, S. Tonegawa, R. Okazaki, H. Shishido, H. Ikeda, H. Takeya, K. Hirata, T. Terashima, and Y. Matsuda, *Evolution from non-Fermi-to Fermi-liquid transport via isovalent doping in $BaFe_2(As_{1-x}P_x)_2$ superconductors*, Phys. Rev. B **81**, 184519 (2010).
- [5] C. H. Lin, K. R. Shirer, J. Crocker, A. P. Dioguardi, M. M. Lawson, B. T. Bush, P. Klavins, and N. J. Curro, *Evolution of hyperfine parameters across a quantum critical point in $CeRhIn_5$* , Phys. Rev. B **92**, 155147 (2015).
- [6] Y. Nakai, T. Iye, S. Kitagawa, K. Ishida, H. Ikeda, S. Kasahara, H. Shishido, T. Shibauchi, Y. Matsuda, and T. Terashima, *Unconventional superconductivity and antiferromagnetic quantum critical behavior in the isovalent-doped $BaFe_2(As_{1-x}P_x)_2$* , Phys. Rev. Lett. **105**, 107003 (2010).
- [7] S. Kitagawa, T. Kawamura, K. Ishida, Y. Mizukami, S. Kasahara, T. Shibauchi, T. Terashima, and Y. Matsuda, *Universal relationship between low-energy antiferromagnetic fluctuations and superconductivity in $BaFe_2(As_{1-x}P_x)_2$* , Phys. Rev. B **100**, 060503 (2019).
- [8] S. Khim, J. F. Landaeta, J. Banda, N. Bannor, M. Brando, P. M. R. Brydon, D. Hafner, R. Kuchler, R. Cardoso-Gil, U. Stockert, A. P. Mackenzie, D. F. Agterberg, C. Geibel, and E. Hassinger, *Field-induced transition within the superconducting state of $CeRh_2As_2$* , Science **373**, 1012 (2021).
- [9] T. Yoshida, M. Sigrist, and Y. Yanase, *Pair-density wave states through spin-orbit coupling in multilayer superconductors*, Phys. Rev. B **86**, 134514 (2012).
- [10] K. Nogaki, A. Daido, J. Ishizuka, and Y. Yanase, *Topological crystalline superconductivity in locally noncentrosymmetric $CeRh_2As_2$* , Phys. Rev. Res. **3**, L032071 (2021).
- [11] C. Lee and S. B. Chung, *Linear optical response from the odd-parity Bardasis-Schrieffer mode in locally noncentrosymmetric superconductors*, Commun. Phys. **6**, 307 (2023).
- [12] A. L. Szabó, M. H. Fischer, and M. Sigrist, *Effects of nucleation at a first-order transition between two superconducting phases: Application to $CeRh_2As_2$* , Phys. Rev. Res. **6**, 023080 (2024).
- [13] D. Hafner, P. Khanenko, E.-O. Eljaouhari, R. Kuchler, J. Banda, N. Bannor, T. Lühmann, J. F. Landaeta, S. Mishra, I. Sheikin, E. Hassinger, S. Khim, C. Geibel, G. Zwicknagl, and M. Brando, *Possible quadrupole density wave in the superconducting Kondo lattice $CeRh_2As_2$* , Phys. Rev. X **12**, 011023 (2022).
- [14] J. F. Landaeta, P. Khanenko, D. C. Cavanagh, C. Geibel, S. Khim, S. Mishra, I. Sheikin, P. M. R. Brydon, D. F. Agterberg, M. Brando, and E. Hassinger, *Field-Angle Dependence Reveals Odd-Parity Superconductivity in $CeRh_2As_2$* , Phys. Rev. X **12**, 031001 (2022).
- [15] K. Semeniuk, D. Hafner, P. Khanenko, T. Lühmann, J. Banda, J. F. Landaeta, C. Geibel, S. Khim, E. Hassinger, and M. Brando, *Decoupling multiphase superconductivity from normal state ordering in $CeRh_2As_2$* , Phys. Rev. B **107**, L220504 (2023).
- [16] S. Mishra, Y. Liu, E. D. Bauer, F. Ronning, and S. M. Thomas, *Anisotropic magnetotransport properties of the heavy-fermion superconductor $CeRh_2As_2$* , Phys. Rev. B **106**, L140502 (2022).
- [17] D. S. Christovam, M. Ferreira-Carvalho, A. Marino, M. Sundermann, D. Takegami, A. Melendez-Sans, K. D. Tsuei, Z. Hu, S. Rößler, M. Valvidares, M. W. Haverkort, Y. Liu, E. D. Bauer, L. H. Tjeng, G. Zwicknagl, and A. Severing, *Spectroscopic Evidence of Kondo-Induced Quasiquartet in $CeRh_2As_2$* , Phys. Rev. Lett. **132**, 046401 (2024).
- [18] B. Schmidt and P. Thalmeier, *Anisotropic magnetic and quadrupolar H - T phase diagram of $CeRh_2As_2$* , Phys. Rev. B **110**, 075154 (2024).
- [19] K. Miyake and A. Tsuruta, *A Possible Scenario for the Anomalous Temperature Dependence of the Resistivity and the Specific Heat of $CeRh_2As_2$ above the Superconducting Transition Temperature and an Origin of the Phase Transition at $T = T_0$* , J. Phys. Soc. Jpn. **93**, 074702 (2024).
- [20] M. Kibune, S. Kitagawa, K. Kinjo, S. Ogata, M. Manago, T. Taniguchi, K. Ishida, M. Brando, E. Hassinger, H. Rosner, C. Geibel, and S. Khim, *Observation of antiferromagnetic order as odd-parity multipoles inside the superconducting phase in $CeRh_2As_2$* , Phys. Rev. Lett. **128**, 057002 (2022).
- [21] S. Ogata, S. Kitagawa, K. Kinjo, K. Ishida, M. Brando, E. Hassinger, C. Geibel, and S. Khim, *Parity transition of spin-singlet superconductivity using sublattice degrees of freedom*, Phys. Rev. Lett. **130**, 166001 (2023).
- [22] K. Machida, *Violation of Pauli-Clogston limit in the heavy-fermion superconductor $CeRh_2As_2$: Duality of itinerant and localized $4f$ electrons*, Phys. Rev. B **106**, 184509 (2022).

- [23] A. Amin, H. Wu, T. Shishidou, and D. F. Agterberg, *Kramers' degenerate magnetism and superconductivity*, Phys. Rev. B **109**, 024502 (2024).
- [24] A. Szabo and A. Ramires, *Superconductivity-induced improper orders in nonsymmorphic systems*, Phys. Rev. B **110**, L180503 (2024).
- [25] G. Chajewski and D. Kaczorowski, *Discovery of Magnetic Phase Transitions in Heavy-Fermion Superconductor CeRh₂As₂*, Phys. Rev. Lett. **132**, 076504 (2024).
- [26] S. Khim, O. Stockert, M. Brando, C. Geibel, C. Baines, T. J. Hicken, H. Leutkens, D. Das, T. Shiroka, Z. Guguchia, and R. Scheuermann, *Coexistence of local magnetism and superconductivity in the heavy-fermion CeRh₂As₂ revealed by μ SR studies*, arXiv preprint arXiv:2406.16575, (2024).
- [27] G. Chajewski, D. Szymański, M. Daszkiewicz, and D. Kaczorowski, *Horizontal flux growth as an efficient preparation method of CeRh₂As₂ single crystals*, Mater. Horiz. **11**, 855 (2024).
- [28] S. Kitagawa, M. Kibune, K. Kinjo, M. Manago, T. Taniguchi, K. Ishida, M. Brando, E. Hassinger, C. Geibel, and S. Khim, *Two-dimensional XY-type magnetic properties of locally noncentrosymmetric superconductor CeRh₂As₂*, J. Phys. Soc. Jpn. **91**, 043702 (2022).
- [29] S. Ogata, S. Kitagawa, K. Kinjo, M. Kibune, K. Ishida, M. Brando, E. Hassinger, C. Geibel, and S. Khim, *Investigation of the hyperfine coupling constant of locally noncentrosymmetric heavy-fermion superconductor CeRh₂As₂*, New Phys.: Sae Mulli. **73**, 1115 (2023).
- [30] K. Ishida, M. Manago, K. Kinjo, and Y. Maeno, *Reduction of the 17O Knight shift in the superconducting state and the heat-up effect by NMR pulses on Sr₂RuO₄*, J. Phys. Soc. Jpn. **89**, 034712 (2020).
- [31] H. Fujibayashi, G. Nakamine, K. Kinjo, S. Kitagawa, K. Ishida, Y. Tokunaga, H. Sakai, S. Kambe, A. Nakamura, Y. Shimizu, Y. Homma, D. Li, F. Honda, and D. Aoki, *Superconducting order parameter in UTe₂ determined by Knight shift measurement*, J. Phys. Soc. Jpn. **91**, 043705 (2022).
- [32] K. Momma and F. Izumi, *VESTA 3 for three-dimensional visualization of crystal, volumetric and morphology data*, J. Appl. Crystallogr. **44**, 1272 (2011).
- [33] I. Kojima and M. Kurahashi, *Application of asymmetrical Gaussian/Lorentzian mixed function for X-ray photoelectron curve synthesis*, J. Electron Spectrosc. Relat. Phenom. **42**, 177 (1987).
- [34] T. Chen, H. Siddiquee, Z. Rehfuss, S. Gao, C. Lygouras, J. Drouin, V. Morano, K. E. Avers, C. J. Schmitt, A. Podlesnyak, S. Ran, Y. Song, and C. Broholm, *Quasi-two-dimensional antiferromagnetic spin fluctuations in the spin-triplet superconductor candidate CeRh₂As₂*, Phys. Rev. Lett. (unpublished).
- [35] H. Watanabe and Y. Yanase, *Magnetic hexadecapole order and magnetopiezoelectric metal state in Ba_{1-x}K_xMn₂As₂*, Phys. Rev. B **96**, 064432 (2017).
- [36] S. Sumita and Y. Yanase, *Superconductivity in magnetic multipole states*, Phys. Rev. B **93**, 224507 (2016).
- [37] N. A. Spaldin, M. Fechner, E. Bousquet, A. Balatsky, and L. Nordström, *Monopole-based formalism for the diagonal magnetolectric response*, Phys. Rev. B **88**, 094429 (2013).
- [38] H. Watanabe and Y. Yanase, *Group-theoretical classification of multipole order: Emergent responses and candidate materials*, Phys. Rev. B **98**, 245129 (2018).
- [39] P. G. de Gennes: *Superconductivity of metals and alloys* (CRC Press, 2018).